

## Simulation of Powder Compaction using Equal Channel Angular Extrusion at Room Temperature: Comparison of Two Constitutive Theories

Anshul Kaushik, Ibrahim Karaman and Arun R Srinivasa\*

*Department of Mechanical Engineering, Texas A & M University, College Station, Texas 77843. USA*

### Abstract:

The process of powder compaction through Equal Channel Angular Extrusion (ECAE) at room temperature was modeled using the finite element analysis package ABAQUS. Two powder compaction models, the Gurson model and the Duva and Crow model, were used to test their efficacy in modeling this process. Modeling parameters like friction coefficients, interaction conditions were determined by comparing the simulations for solid billet and an empty can with actual experimental runs for loads, shear angle and workpiece geometry. The simulations using the two models showed no significant difference in the stress in the powder during the extrusion. 2-D simulations were used to show the efficacy of two passes of ECAE in achieving full densification in the extruded workpiece. The results obtained from the simulations were also compared to experiments conducted to compact copper powder with a size distribution of 10 $\mu$ m to 45 $\mu$ m. It was found through experiments that the powder does not fully consolidate near the outer corner of the workpiece after the first ECAE pass and the results from the simulations were used to rationalize this phenomenon. Modifications made to the process by applying a back pressure during the simulations resulted in a uniformly compacted powder region. It was also found that the loads required to consolidate a powder through ECAE are much lower than conventional pressing or compression to achieve the same amount of compaction.

**Keywords:** Equal Channel Angular Extrusion, Equal Channel Angular Pressing, Powder compaction, Constitutive behavior, Finite elements.

### 1. Introduction

In recent years, Equal Channel Angular Extrusion (ECAE), also called Equal Channel Angular Pressing (ECAP) has developed as a method to produce ultra fine-grained materials (Segal, 1995). It is effectively a method to produce a large amount of simple shear deformation in a material by passing it around a corner of two intersecting channels with equal cross-sections as seen in Figure 1. The main advantage of ECAE over conventional extrusion is that the cross section of the material undergoing ECAE remains the same after the process and thus it can be passed through the same die to repeat the process and accumulate higher plastic deformation (Zhu and Lowe, 2000). In addition, the deformation is quite uniform as compared to that from the conventional deformation processes.

In ECAE, the workpiece which is typically a solid billet is placed in one of the channels and forced to pass into the second channel using a plunger. As the billet passes through, it is severely deformed in shear within a small area at the intersection of the two channels. The mechanical properties and microstructure of several materials undergoing ECAE have been extensively studied and thoroughly summarized in a recent review by Valiev and Langdon (2006). Many studies have been conducted to investigate the unique microstructural features that can be obtained through multiple pass ECAE (Zhu and Lowe, 2000). Work on modeling the ECAE process has been carried out in detail to study the effect of processing parameters like die shape, friction, back pressure in previous works such as those by Luis Perez et al. (2004), Oh and Kang (2003) and Li et al (2004) and the modeling of microstructural evolution during ECAE has been attempted by Beyerlein et al. (2003), Beyerlein et al. (2005), Iwahashi et al. (1997) and Iwahashi et al. (1997).

In the recent past, ECAE has also been used for compaction of powders, mainly by putting the powder in a can and passing the can through an ECAE die (Parasiris et al., 2000; Matsuki et al., 2000; Kim et al., 2003; Robertson et al., 2003; Haouaoui et al., 2004; Karaman et al., 2004; Senkov et al., 2004; Senkov et al., 2005; Xia and Wu, 2005; Karaman et al., 2007).. The key goal of most of these works was to achieve full densification in micron and nanometer

\*Email: asrinivasa@tamu.edu

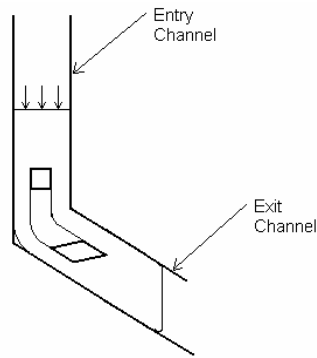


Figure 1. Schematic of the ECAE process showing the deformation of an element of the workpiece during ECAE.

sized powders without coarsening, to obtain truly bulk nanocrystalline materials, fabricate bulk metallic glasses, microstructural design and mechanical property enhancement. The compaction of powders with ECAE at low temperatures makes it possible to fabricate bulk materials with grain size from nano to micron size scale (Haouaoui et al., 2004; Xia and Wu, 2005; Karaman et al., 2007). The benefit of powder compaction by ECAE is effective consolidation at lower temperatures than normally required by Hot Isostatic Pressing (HIP) operations. ECAE processing is especially attractive for making bulk nanocrystalline materials because of 1: The possibility of consolidation below dynamic recovery temperatures, 2: Large product cross sections and 3: Easy incorporation of second phase components (other powders, filamentary or rod dispersoids) which are not suitable for incorporation during a melting step.

There is a definite need for a computational process design approach which requires an accurate approximation for the materials constitutive behavior. Finite Element analysis of metallic powders undergoing ECAE has been carried out in a previous work by Yoon and Kim (2006). They showed, through their simulations that hydrostatic pressure is first developed in the entry channel which assists the compaction and then simple shear is generated as the sample passes through the corner. Their results predicted that the powder solidifies fully before it enters the corner and the deformation in the corner is simple shear. These 2-D simulations, without a material can, are not adequate to capture the true nature of a powder compaction through ECAE because the powder can has a substantial effect on the mechanics of compaction as a way to control the hydrostatic pressure.

This paper reports the modeling effort on the densification of copper powder through ECAE at room temperature by using two different powder compaction models: The Gurson model (Gurson, 1977) and the Duva and Crow model (Duva and Crow, 1992) in the finite element analysis carried out using ABAQUS/Explicit (Abaqus Inc, 2004). 2-D and 3-D simulations are carried out in order to point out the inadequacies of the 2-D simulations. The densification behavior, kinematics of the deformation and the stresses developed are studied to analyze certain characteristics observed during the compaction experiments. The efficacy of applying back pressure during compaction is demonstrated in achieving fully dense powder compacts.

## 2. Powder compaction models

Many powder compaction models and consolidation mechanisms have been proposed to suitably model the various methods like sintering, hot isostatic pressing, area reduction extrusion and cladding processes (Gurson, 1977; Duva and Crow 1992; Wilkinson and Ashby, 1975; Tvergaard, 1981; Carroll, 1986; Kim and Carroll, 1987; Kim and Suh, 1990; Delo and Piehler, 1999). In this paper, the powder models used are the Gurson model, which is built into the ABAQUS package and the Duva and Crow model, for which a user material subroutine (VUMAT) is implemented to be used with the ABAQUS finite element model.

### 2.1. Gurson model

The Gurson model (1977) accounted for the plastic dilatancy which is characteristic to porous ductile materials and thus showed the importance of hydrostatic pressure in the yield condition for such materials. The theory was developed by idealizing the void-matrix aggregate to a single void in a cell in which the volume of the void is equal to the void

volume fraction in a unit cell. The cell is presumed to have rigid plastic properties. Two void geometries were considered: spherical voids in a spherical matrix and long cylindrical voids in cylindrical matrix. Proceeding with this configuration, a yield condition was proposed as

$$\Phi = \left(\frac{q}{\sigma_y}\right)^2 + 2f \cosh\left(\frac{-3P}{2\sigma_y}\right) - (1 + f^2) \quad (1)$$

where,  $P = -\frac{1}{3}\underline{\sigma} \cdot \underline{I}$  is the negative mean normal stress,  $\underline{S} = P\underline{I} + \underline{\sigma}$  is the deviatoric part of the stress with  $q = \sqrt{\frac{3}{2}\underline{S} \cdot \underline{S}}$

and ' $f$ ' is the void volume fraction (porosity).

The plastic strain is evaluated through

$$\dot{\underline{\epsilon}}^p = \lambda \frac{\partial \Phi}{\partial \underline{\sigma}} = \lambda \left( \frac{-1}{3} \frac{\partial \Phi}{\partial p} \underline{I} + \frac{3}{2q} \frac{\partial \Phi}{\partial q} \underline{S} \right) \quad (2)$$

and the void volume fraction ' $f$ ' is given by

$$\dot{f} = (1 - f) \text{tr}(\dot{\underline{\epsilon}}^p) \quad (3)$$

The elastic constitutive behavior is given by

$$\Delta \underline{\sigma} = \underline{E} : \Delta \underline{\epsilon}^{el} = \underline{E} : (\Delta \underline{\epsilon} - \Delta \underline{\epsilon}^p) \quad (4)$$

where  $\underline{\epsilon}$  is the logarithmic strain, defined as  $\underline{\epsilon} = \frac{1}{2} \ln(\underline{F}\underline{F}^T)$ ,  $\underline{F}$  being the deformation gradient tensor.

This elastic constitutive equation (4) is solved by utilizing a backward Euler scheme. The total incremental strain from the previous time step is utilized to update the stress, the plastic strain and the void volume fraction at the next time step so that they satisfy the yield condition (1), flow rule (2) and evolution of void volume fraction (3).

It should be noted that when  $f$  goes to zero, the material is fully dense and thus the model reduces to the von Mises theory for elastic-plastic materials. It should also be noted that the material would soften in tension because of opening of the voids and harden in compression due to closing of the voids. This model overpredicts the stresses during a compaction process when compared to other models as shown by Biswas (2005) and is thus generally found unsuitable to model powder compaction where the initial relative density of the powder is below 0.9 (Abaqus Inc, 2004).

## 2.2. Duva and Crow model

Duva and Crow originally suggested a model to study the densification of powders undergoing Hot Isostatic Pressing (1992). This model has since been used since to study the powder compaction process by Carmai and Dunne (2004) and Carmai and Dunne (2005).

The Duva and Crow model accounts for both the deviatoric and hydrostatic stresses to model the compaction process. The model assumes that the powder material is incompressible and nonlinearly viscous. A strain rate potential for a porous, non-linear creeping material is used and the densification rate is computed by differentiating this strain rate potential by the stress. The strain rate potential is given by

$$\phi = \frac{\dot{\epsilon}_0 \sigma_0}{n+1} \left( \frac{S}{\sigma_0} \right)^{n+1} \quad (5)$$

Where  $\dot{\epsilon}_0$  and  $\sigma_0$  are any convenient reference strain rate and stress, respectively and  $n$  is the creep exponent, used for the powder material. Each of these parameters is, in general, dependent on the temperature.

The stress measure ( $S$ ) proposed in this model is given by

$$S^2 = a\sigma_c^2 + b\sigma_m^2 \quad (6)$$

where,

$$\sigma_c^2 = \frac{3}{2} \underline{\tau} \cdot \underline{\tau} \text{ is the effective stress, } \underline{\tau} \text{ is deviatoric part of the stress,}$$

$$\sigma_m = \frac{1}{3} \text{tr}(\underline{\sigma}) \text{ is the hydrostatic pressure and } n \text{ is the creep exponent.}$$

The variables  $a$  and  $b$  depend on the Relative Density ( $RD$ ) and are given by:

$$a = \frac{1 + (2/3)(1 - RD)}{RD^{2n/(n+1)}} \tag{7}$$

$$b = \left[ \frac{n(1 - RD)}{(1 - (1 - RD)^{1/n})^n} \right]^{2/(n+1)} \left( \frac{3}{2n} \right)^2 \tag{8}$$

The Jaumann stress rate is given by

$$\overset{\nabla}{\sigma} = 2\mu D^{el} + \lambda tr(D^{el}) I \tag{9}$$

where  $D^{el}$  is given by the additive decomposition of the symmetric part of the velocity gradient as

$$D^{el} = \underline{D} - D^p \tag{10}$$

and the increment in stress is given by

$$\Delta \sigma = \Delta \overset{\nabla}{\sigma} + \underline{R} \sigma \underline{R}^T \tag{11}$$

The plastic strain rate  $D^p$  can be determined from the strain rate potential (5) by differentiating it with respect to the stress  $\sigma$  which gives,

$$D^p = \frac{\partial \phi}{\partial \sigma} = AS^{n-1} \left( \frac{3}{2} a \underline{\tau} + \frac{1}{3} b \sigma_m I \right) \tag{12}$$

Where  $A$  is defined by

$$A = \frac{\dot{\epsilon}_0}{\sigma_0^n}$$

The dilatation rate is given by  $tr(D^p)$  and the rate of change of relative density is given by

$$\dot{RD} = -RD tr(D^p) \tag{13}$$

A first order forward Euler integration scheme is adopted and the constants  $a$  and  $b$ , the stress, plastic strain rate and the relative density, are updated through (7), (8), (11), (12) and (13) respectively. The symmetric part of velocity gradient  $\underline{D}$  and the rotation tensor  $\underline{R}$  from the previous time step are taken to update these variables.

The model introduces the relative density dependent parameters  $a$  and  $b$  so that the effect of pressure on the measure of yield stress vanishes when the powder is fully consolidated. The variation of  $a$  and  $b$  with the relative density is shown in the Figure 2.

In order to determine the appropriate constant  $A$  and the creep exponent  $n$  which are used with the model, we compare the Duva and Crow model with the Gurson model in pure compression and simple shear for a medium with an initial relative density of 0.9. It should be noted that the form of the yield conditions used in the two models are significantly different from each other, one having trigonometric terms and other being purely polynomial. Another key difference is that the base material is rigid-plastic in the Gurson model whereas it is nonlinearly viscous in the Duva and Crow model.

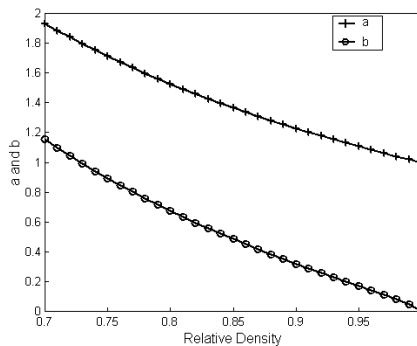


Figure 2. Variation of variables  $a$  and  $b$  with relative density. It can be noted that  $a$  goes to 1 and  $b$  goes to 0 as relative density goes to 1 giving the Von Mises criterion.

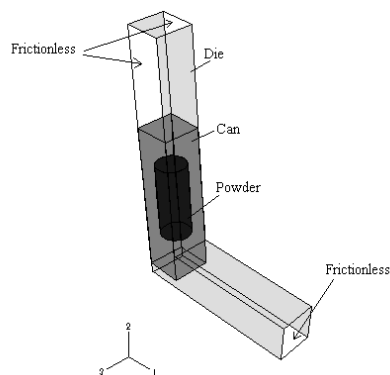


Figure 3. 3-D Schematic of the ECAE die with a can and powder. The surfaces where the die walls slide with the can are shaded lighter in color and marked frictionless.

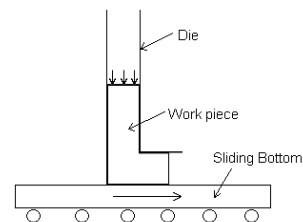


Figure 4. Schematic of the ECAE process. Note that the bottom slides with the work piece.

### 3. Details of the experiments and modeling

#### 3.1. Experiments

The experiments were carried out for compacting micron sized copper powder with a size distribution of  $10\mu\text{m}$  to  $45\mu\text{m}$  using ECAE by placing it in a pure copper can. The can and die used in the experiments are of square cross section with 2.5 cm side. The can has a hole of 2 cm diameter in the center which was filled with the powder. The total length of the can is 10 cm and the hole is of length 5 cm and are schematically shown in Figure 3. During the extrusion, the bottom portion of the die and the side walls of the inlet channel slide with the work piece undergoing the extrusion to reduce the friction. This arrangement is schematically shown in Figure 4. It should be noted that these extrusions were carried out at room temperature to prevent dynamic recovery/ recrystallization and grain growth.

Figure 5 shows the section of the extruded can with powder after 1 ECAE pass, sliced longitudinally from the center, where the region containing the powder is demarcated using the dotted line. It should be noted here that in the results section for the 3-D simulations, only the region containing the powder, bound by the dotted line will be shown. It can be seen that the bottom portion of the powder is not fully compacted. Also through Optical microscopy, the shear angle of the compacted powder was determined to be 26.4 degrees.

#### 3.2. Finite Element Simulations

The 2-D and 3-D Finite element simulations for the ECAE process were performed using the finite element package ABAQUS/Explicit (Abaqus Inc., 2004). The model consists of three key components, the die, the can and the powder core as seen in Figure 3. Details regarding the material constitutive equations, boundary conditions and surface interactions etc are provided in the subsequent sections.

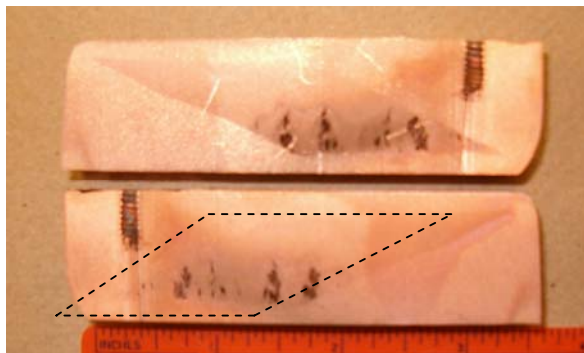


Figure 5. Middle section of extruded can with powder. The compacted powder is marked with the dotted outline.

### 3.2.1. Material properties

The ECAE die is modeled using a rigid surface. For the copper can, a linear hardening elastic-plastic material model is used with Young's modulus of 124 GPa, initial yield stress of 80 MPa which hardens to 300MPa. For the powder, the two models described earlier are implemented. The Gurson model is built into ABAQUS. To implement the Duva and Crow model, the user subroutine VUMAT (Abaqus Inc., 2004) is used. In both these powder models, the same material properties of copper are used.

### 3.2.2. Surface Interactions

Two key interactions need to be modeled in these simulations, namely the interactions between the can and the die and between the can and the powder. The interaction between the can and the powder is modeled using hard contact and forcing the condition that the powder sticks to the can material. In the tangential direction, frictionless contact is assumed. This seems reasonable because macroscopically, there is very little relative motion between the can and the micron size powder.

In the case of the interaction between the can and the die, for the faces where the walls of the die slide with the work piece, a zero coefficient of friction is assumed. On all other walls, a friction value of 0.08 is applied. This value was determined by running the 3-D simulations for a solid billet and then comparing the macroscopic properties of the billet and the loads applied at the punch obtained from these simulations to those observed during the experiments. This is described in detail in the "validation" section. In the normal direction, the contact is modeled so that the can material is free to detach from the die material after coming into contact.

### 3.2.3. Extrusion Rate

The experiments were conducted at an extrusion rate of approximately 0.1 in/s. For a regular dynamic explicit integration scheme, simulations at this rate would take very large computational times. To reduce the convergence time associated with such simulations, we introduce the concept of mass scaling in our model. The concept of mass scaling has been used in the past (Olovsson et al., (2005); Smith et al., 2004) to reduce convergence times in explicit finite element simulations. A mass scaling factor of 100 is used in the simulations. This choice is made so that the inertial effects due to the mass scaling do not affect the results of the simulations.

### 3.2.4. Validation

A key step is to validate the finite element model with the experiments, to assure that the boundary conditions (such as the friction coefficients, the contact conditions etc) and the constitutive model for the solid material are reasonable. These validations were performed for the extrusions with a solid billet. A copper billet with an original rectangular grid inscribed at the center of the billet after splitting the billet longitudinally into two was extruded through ECAE. The corner angles this grid made after the extrusion were compared to the angle made by the simulated elements of the mesh. In addition, the major geometric parameters such as final length, shape and the punch load etc were compared. Another step in the validation was to extrude an empty can (without the powder) and compare the experimental shapes to the simulations. With these steps, the boundary conditions were optimized and it was determined that the boundary conditions and constitutive equations for the solid material described earlier were reasonable.

### 3.2.5. Back Pressure

Back pressure technique is a modification to the ECAE process where a counter pressure is applied to the leading edge of the workpiece as it emerges out of the exit channel. This method has been used to achieve better workability and more uniform microstructures in bulk billets as presented by Stolyarov and Lapovok (2003). Simulations using back pressure have been performed and have shown that back pressure produces higher and more uniform shear strains in bulk materials (Oruganti et al., 2005).

### 3.2.6. Multiple Passes

A key advantage of ECAE is that the cross section of the workpiece does not change after the extrusion. Thus it can be extruded again through the same die multiple times to accumulate higher and higher plastic strains. This process has been shown as an effective way to achieve strain hardening and accumulate higher plastic strains in bulk materials, through simulations by Baik et al. (2003). During powder compaction through ECAE, it has been shown as an effective

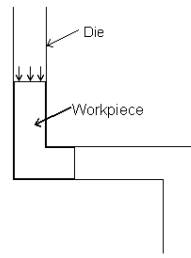


Figure 6. Die design for 2-Pass ECAE with  $180^{\circ}$  rotation of the workpiece about the longitudinal axis.

means to achieve full compaction. A comprehensive study by Karaman et al. (2006) has shown that a 2 pass ECAE to consolidate powders not only gives better consolidation but also considerably affects the material characteristics of the consolidated solid. The effect of 2 passes will be studied here through 2-D simulations. The die designed to simulate the multiple passes is shown in Figure 6. In the first step the top surface is given a downward velocity and in the second step, the surface to the left is given a horizontal velocity to the right. This motion is equivalent to rotating the workpiece by  $180^{\circ}$  about its central axis and passing it through the die again for the second pass.

### 3.2.7. 2-D simulations

The main goal of the 2-D simulations is to compare the results obtained from the two powder constitutive models and to compare the same with the results from other literature. The 2-D simulations are carried out using the plane strain condition. The simulation was done considering a work piece consisting entirely of the powder material. This is not possible practically because without a container the powder will flow, but the theories considered here assign tensile strength to the powder material. This situation is almost equivalent to putting the powder in a thin walled can and passing it through the ECAE die. The can was not considered in these simulations to reduce the computation cost required due to the additional interaction between the can and the powder.

### 3.2.8. 3-D simulations

The key goal of the 3-D simulations is to model the powder compaction through ECAE process accurately and to study the kinematics and stress states during the compaction process in detail. The results from the simulations can be used to explain some of the phenomena observed in the compaction experiments.

## 4. Results

### 4.1. 2-D simulation results

The main purpose of the 2-D simulations was to study the efficacy of the powder material constitutive models to model the ECAE process under relatively simple simulation conditions. In these simulations, we started with a powder of relative density of 0.8. The key results discussed in this section are the comparison of the kinematics and the stresses obtained from the 2 constitutive models as the work piece is extruded.

Figures 7 and 8 show that both models predict almost full densification is achieved near the inner corner of the intersecting channels. The densification profile and the final shape of the work piece are similar for both models. It should be noted that in Figure 7, Void volume fraction is plotted whereas in Figure 8, Relative density is plotted (It should be noted that the color codes in both the figures correspond to same relative density). To further study the stress states in the material and compare them for the two constitutive theories, we select an element from the mesh which is about at the center of the work piece. For this element, we track its volume, the relative density and the stresses as it undergoes the extrusion. Figure 9 shows the sequence of the configurations of the work piece as it passes through the die. The element that is selected for analysis is marked in dark.

From Figure 10a, we can see that the volume of the element decreases continuously until it passes through the corner completely. Once it passes through the corner, there is no change in the volume after the powder enters the exit channel and the material does not consolidate further as also seen from Figure 10b. The reason for consolidation before entering the bend is clear from Figures 11a and 11b where we can see that a high hydrostatic pressure is built in the material before it enters the corner zone.

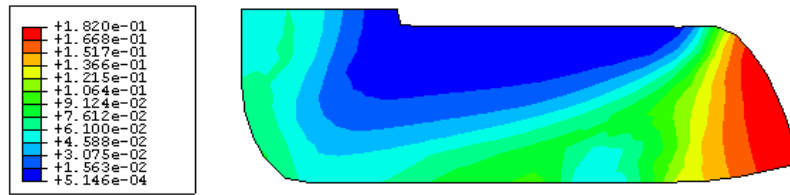


Figure 7. Final shape and contours of the Void Volume Fraction – Gurson Model. The dark blue regions are fully consolidated and the red region shows least consolidation.

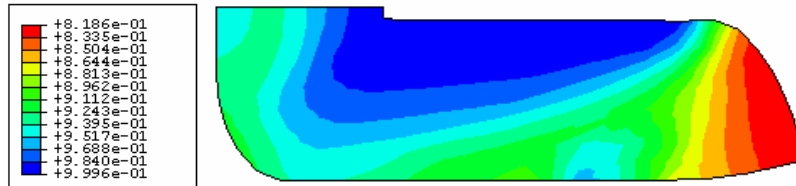


Figure 8. Final Shape and Contour for Relative Density – Duva and Crow Model. The dark blue regions are fully consolidated and the red region shows least consolidation.

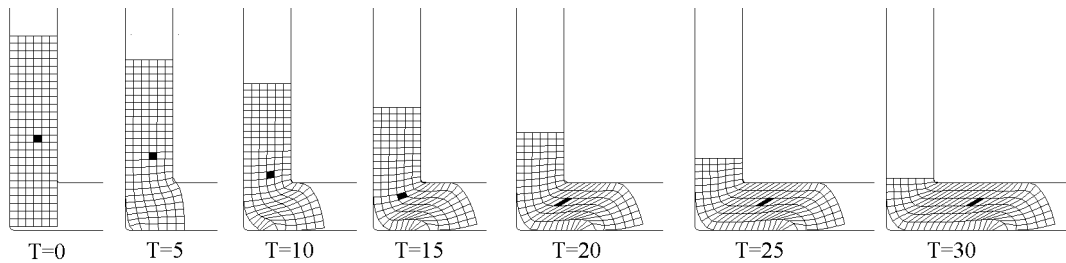


Figure 9. Sequence of the shape evolution of 2-D powder medium during the ECAE predicted using Duva and Crow model (selected element is marked dark). T=0 is the initial state of the workpiece and T=30 is fully extruded.

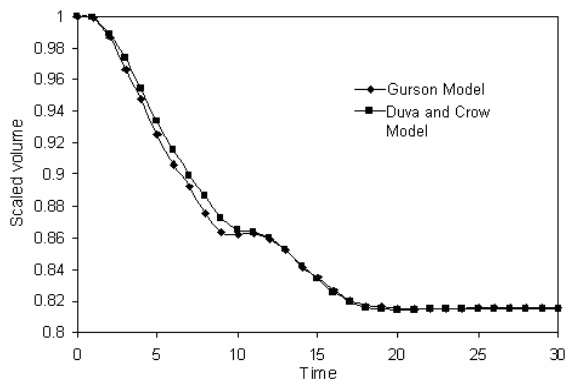


Figure 10a. Volume of the selected Element with initial volume scaled to 1. It can be seen that most of the change in volume takes place before the element enters the bend ( $T < 10$ ) and no consolidation takes place after it has passes through ( $T > 20$ )

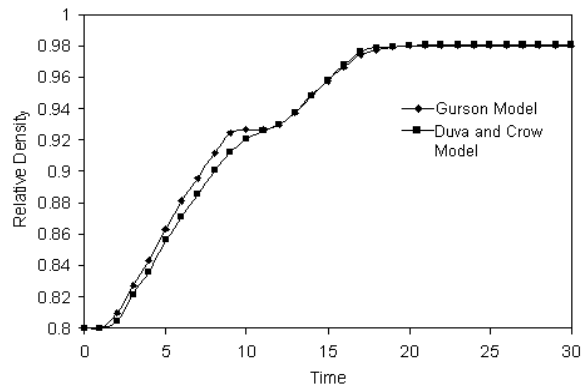


Figure 10b. Relative Density of the selected element. It can be seen that most of the consolidation takes place before the element enters the corner ( $T < 10$ ) and no consolidation takes place after it has passes through the corner region ( $T > 20$ )

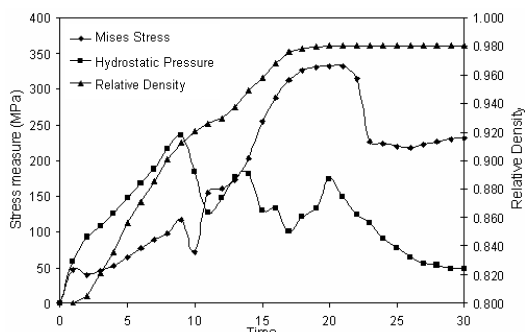


Figure 11a. Mises stress, hydrostatic pressure (negative mean normal stress) and relative density (the Gurson model). It can be seen that a high hydrostatic pressure is developed before the element passes through the corner, resulting in most of the consolidation.

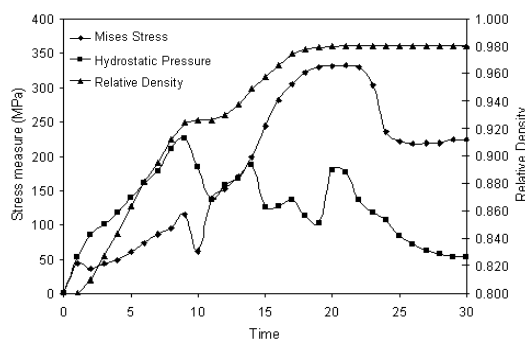


Figure 11b. Mises stress, hydrostatic pressure (negative mean normal stress) and relative density (Duva and Crow model). It can be seen that a high hydrostatic pressure is developed before the element passes through the bend, resulting in most of the consolidation.

From these figures, it is clear that both models predict similar stress response for the powder. Although there are subtle differences in the stress and relative density predictions, the stresses conditions in the material leading to consolidation are the same.

In the previous literature, Yoon and Kim (2006) had shown through simulations that the powder solidifies fully before it enters the corner and the deformation in the corner is simple shear. On the other hand, our 2-D simulations show that the powder does not fully compact before it enters the entry channel especially around the bottom portion of the work piece. This result is encouraging because the experiments showed similar uncompacted region in the bottom region of the powder compact.

#### 4.2. Results for two passes

Figure 12 shows the contours for the relative density obtained through a 2-D simulation starting with a relative density of 0.8. The contour after 1 pass is shown in Figure 8. It can be seen that the whole region (except the two ends) is fully consolidated. Figure 13a shows the deformed elements after 2-Pass ECAE. The elements (away from the ends) tend to go back to their original rectangular shape because of reversal of the shear strains, but the original rectangular grid is not obtained because of combined compression with the shear deformation. Figure 13b shows the deformation of the workpiece at an intermediate time step while undergoing the second pass. Notice that the shear in the elements is reversed in the shear deformation zone.

In Figure 14, the relative density of an element is plotted with respect to time. The element for which the relative density is plotted is marked in gray in Figure 13a. It can be seen that the material in the element is only partially consolidated at the end of the first pass and then consolidates fully during the second pass. The first pass is represented by the first 30 seconds in the time scale and the second pass is on the 31-60 seconds. Notice that during the second pass, the material in the element does not start consolidating immediately, which is unlike the first pass where the material starts consolidating as soon as the workpiece starts extruding. The material consolidates only when the element passes through the shear zone.

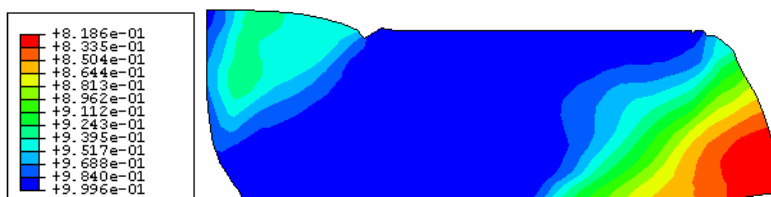


Figure 12. Final Shape and Contour for Relative Density obtained from the Duva and Crow Model after two passes. The dark blue regions are fully consolidated and the red region shows least consolidation.

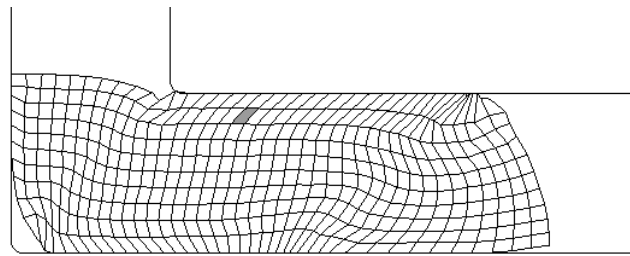


Figure 13a. The deformed elements after 2 passes. Notice the elements away from the ends show an almost complete reversal of the shear.

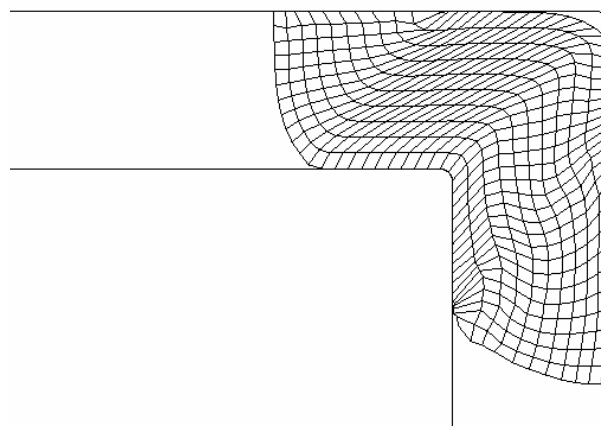


Figure 13b. The extruded workpiece halfway through the second pass. Notice the reversal of shear in the shear zone.

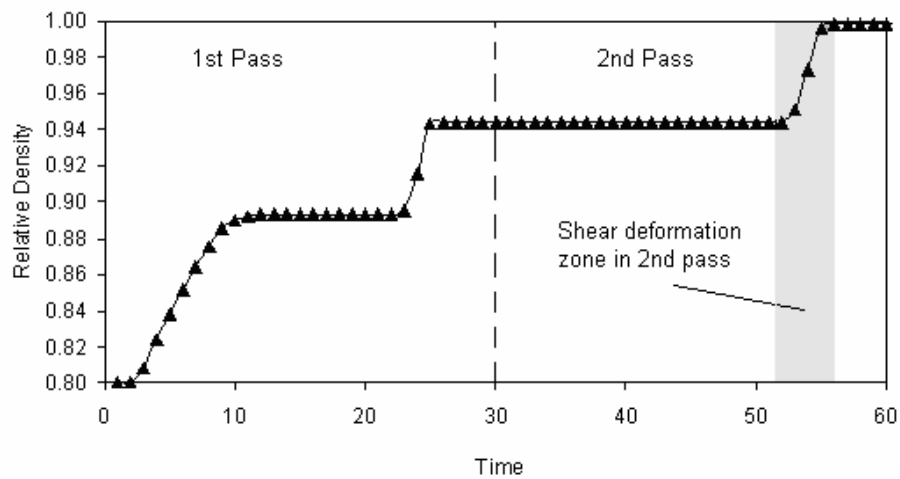


Figure 14. The relative density of a selected element (marked in gray in figure 13a) during the extrusion. Notice in the second pass, the consolidation occurs only in the shear zone.

#### 4.3. 3-D simulation results

To study the powder compaction process in detail, we first try to compare the 3-D simulations with the experiments for verification. For this we compare the distribution of the relative density of the compacted powder macroscopically and the angle by which the particle boundaries shear. After the validation, we try to explore the reasons for the incomplete compaction in certain regions.

Figures 15 and 16 show contours for the void volume fraction and the relative density, respectively, at the middle section of the compacted powder. In these simulation results, we can see that the leading and the back corners of the powder core shows almost no densification. This anomaly might be because of the type of boundary condition applied which requires that the powder stick to the walls of the can. Also in Figure 16 we can see that the Duva and Crow model predicts the location of the unconsolidated cavities more precisely. The angle measured from the OM pictures was 26.4 degrees. The angle obtained from the simulation using the Gurson model is 28.4 degrees and using the Duva and Crow model is 27.6 degrees.

From the Figures 6, 15 and 16, it can be seen that the bottom portion of the powder does not fully consolidate. To further study this phenomenon and make comparisons of the stresses in the top and bottom parts of the powder in the can, we select two respective elements: one from the top (element A) and another from the bottom (element B) from the powder space. For these two elements, using the Duva and Crow model, we plot the stresses and the porosity evolution as they undergo the extrusion. The positions of the two elements at various simulation times are shown in Figure 17.

From Figures 18a and 18b, it is clear that the magnitude of hydrostatic pressure developed before passing through the corner in element A is much higher than the hydrostatic pressure in element B (maximum of 550 MPa compared to 350 MPa). Thus the densification rate is higher in the element A. Also it can be seen that in element B, the powder undergoes very little densification even after it has passed through the corner. The difference in the hydrostatic pressure between elements A and B can be attributed to bending of the can when passing through the bend. Several strategies could be employed to reduce this difference, for example, use of a can of stiffer material, back pressure etc.

#### 4.4. Simulations with Back Pressure

From the results discussed above, it is clear that the lack of compaction in the lower portion of the powder may be because of the lower hydrostatic pressure levels developed in this region. To overcome this, application of back pressure could give adequate hydrostatic pressure to the material in the lower region for complete compaction. The approach to apply back pressure should be chosen in such a way that it is experimentally feasible to apply and leads to the desired results. For this reason a constant back pressure of 200 MPa (which is equal to the difference in the hydrostatic pressure between elements A and B) is applied to the lower region of the workpiece which is schematically shown in Figure 19.

Figure 20 shows the result of the simulation performed using the Duva and Crow model with back pressure applied. It is clear that the powder at the bottom region is fully compacted now as compared to Figure 16, which is the simulation without back pressure. It can also be seen that the bottom portion of the leading edge of the compacted region is pushed back because of the back pressure as compared to the simulation without back pressure shown in Figure 16.

To study the evolution of the stresses in the bottom region, the element B is selected and the stress components are plotted in Figure 21. The hydrostatic pressure developed is not significantly higher than the simulation without back pressure (Figure 18b). But the drop in hydrostatic pressure after passing through the corner is significantly reduced, which results in continued compaction after passing through the corner zone.

#### 4.5. Comparison of loads to compact the powder through ECAE vs. loads through pure compression

At this stage we would like to make a remark on the maximum loads required to carry out the compaction of the powder. In this section, maximum loads required for 3 methods are compared. 1) ECAE without back pressure, 2) ECAE with back pressure and 3) uniaxial compression. The loads required for the former 2 processes are readily available through the simulations carried out, as described in the previous sections. For the 3<sup>rd</sup> process, a routine simulation is carried out, using the Duva and Crow constitutive model for a powder material with the same dimensions as the powder extruded in the can during ECAE.

The maximum load required to carry out the ECAE without back pressure is 298.2 KN. The load during the ECAE with back pressure is 362.4 KN. The load required to compact the powder through compression is 478.7 KN. This shows that the loads required to compact the powder through ECAE are significantly lower than those required during compression.

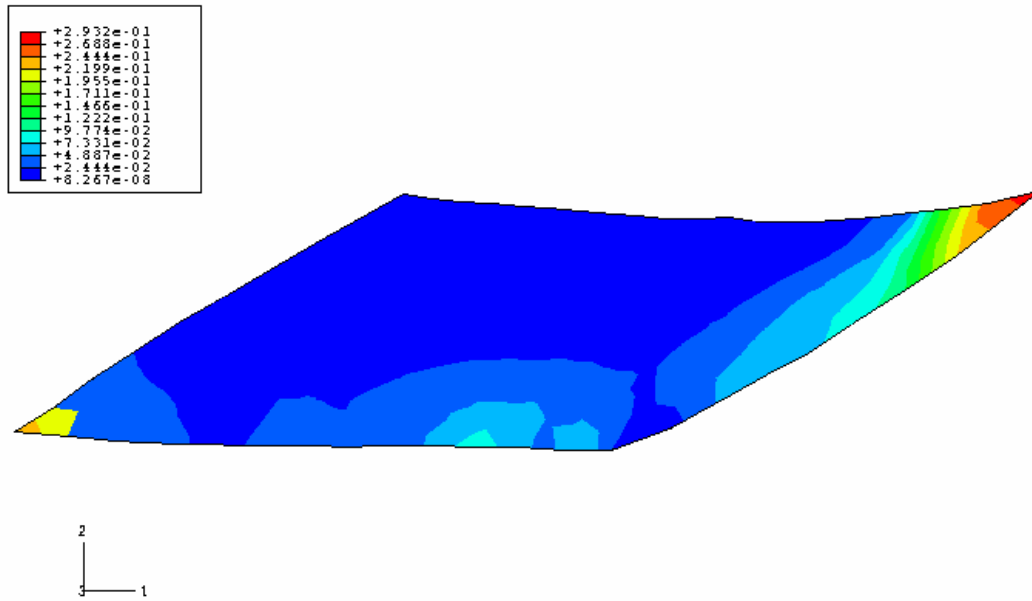


Figure 15. Void Volume Fraction predicted by Gurson model. The dark blue regions are fully consolidated and the red region shows least consolidation.

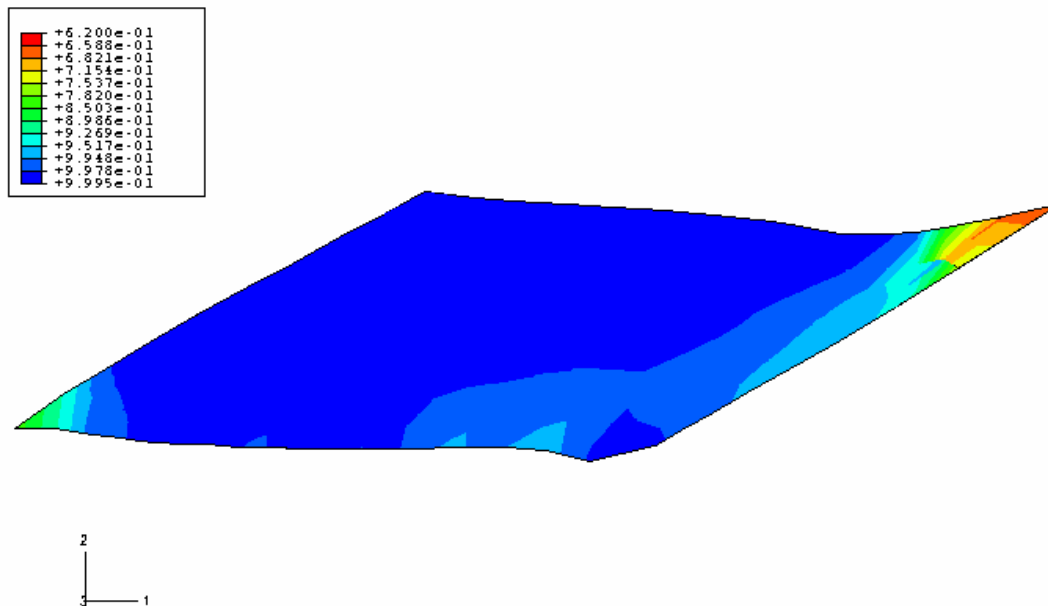


Figure 16. Relative Density predicted by Duva and Crow model. The dark blue regions are fully consolidated and the red region shows least consolidation.

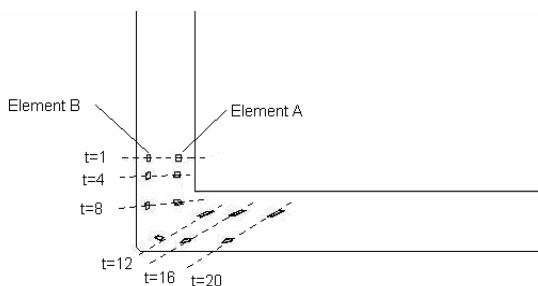


Figure 17. Position of Elements A and B at scaled times 1, 4, 8, 12, 16, 20. T=1 shows the elements as the extrusion starts and T=20 shows the elements when the can is fully extruded.

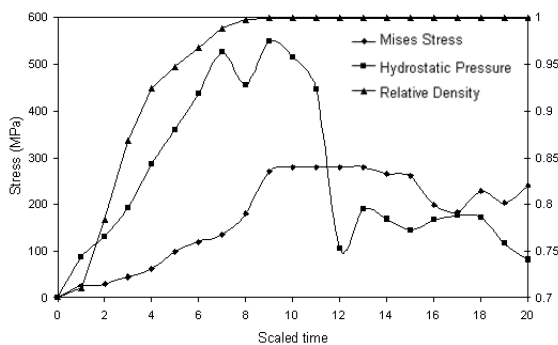


Figure 18a. Mises stress, hydrostatic pressure (Negative Mean Normal stress) and relative density for Element A. It can be seen that a high hydrostatic pressure is developed before the element passes through the corner, resulting in most of the consolidation.

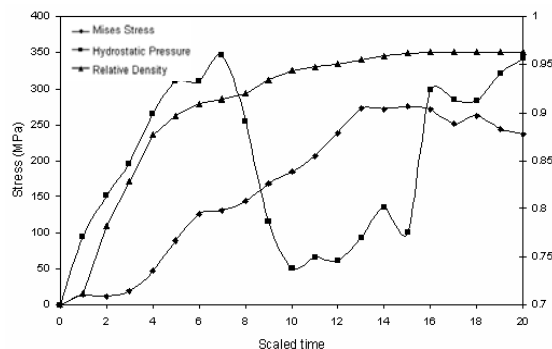


Figure 18b. Mises stress, Hydrostatic pressure (Negative Mean Normal stress) and Relative Density for Element B. It can be seen that a high hydrostatic pressure is developed before the element passes through the bend, resulting in most of the consolidation.

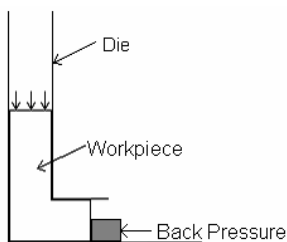


Figure 19. Schematic showing the application of a back pressure to the lower region of the workpiece during extrusion.

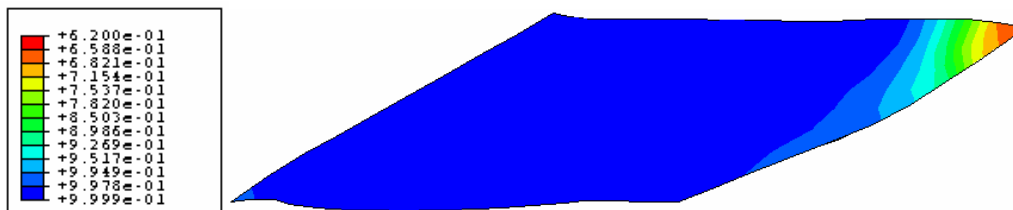


Figure 20. Relative Density predicted by Duva and Crow model for ECAE with Back Pressure. The dark blue regions are fully consolidated and the red region shows least consolidation. It should be noted that we get improved consolidation in the bottom region.

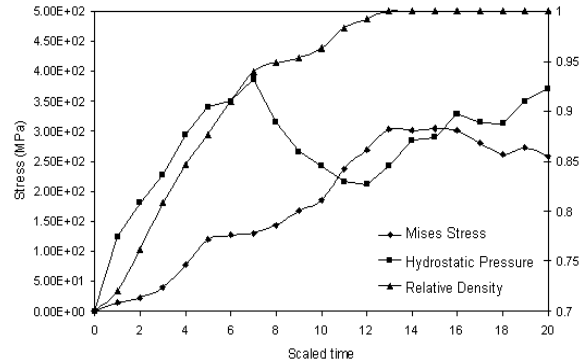


Figure 21. Mises stress, hydrostatic pressure (Negative Mean Normal stress) and relative density for Element B with back pressure. It can be seen that the drop in hydrostatic pressure after passing through the bend is not as significant here as it is without back pressure, resulting in better compaction.

## Conclusions

In the present study, the process of powder compaction through ECAE was simulated using the finite element package ABAQUS. For the constitutive behavior of the powder, two models were implemented, the Gurson model and the Duva and Crow model. The results from the 3-D simulations which mimic the experimental conditions were used to understand the compaction behavior and explore the possibility of improving the compaction by using back pressure in the process. Some key conclusions drawn in the process are listed here.

1: The powder compaction models, Gurson model and the Duva and Crow model, predict similar response for the compaction through ECAE.

2: In the 2-D simulations, we see that the powder near the inner corner consolidates almost completely whereas the powder at the outer corner does not. It is observed that majority of the compaction takes place before the powder enters the bend due to the high hydrostatic pressure developed there. The 2-D simulations are not enough to predict the response of the powder compaction in a can, thus requiring full scale 3-D simulations.

3: Through 2-D simulations, we see that multiple pass ECAE is a very effective way of achieving uniform and complete densification in the center of the workpiece.

4: In the 3-D simulations, the Duva and Crow model predicts the compaction more accurately to the experiments than the Gurson model.

5: From the experiments and the 3-D simulations it can be observed that the powder in the can near the outer edge does not consolidate completely. The reason for this as seen from the simulations is the higher hydrostatic pressure developed near the inner corner.

6: It can be seen through simulations that application of back pressure is an effective means to achieve uniform compaction over the whole region.

Future work using the simulation methodology developed in this work can include carrying out a parametric study to optimize the process design variables like back pressure, friction between the walls of the die and the can, the rate of extrusion, can dimensions and shape, can material and number of passes etc

Another key aspect in understanding the compaction process is to study the bonding between the individual particles, which is a micro scale problem and thus cannot be tackled at this scale. To study the bonding, plastic deformation and diffusion phenomena at the particle level, the displacement and stress results from the simulations in this work at an element level can be used as input to develop microscale models.

## Acknowledgements

The funding for this work came from the National Science Foundation: Materials Processing and Manufacturing Division under Grant No. 0423649 for which the authors are grateful. IK also acknowledges the funding from the Office of Naval Research under Grant No. N00014-05-1-0615 with Dr. Lawrence Kabacoff as program officer.

**References**

- Abaqus Inc., 2004. Abaqus Users Manual, Version 6.5: Abaqus Inc.
- Baik S.C., Estrin Y., Kim H.S., Hellmig R.J., 2003. Dislocation density-based modeling of deformation behavior of aluminium under equal channel angular pressing. *Materials Science and Engineering a-Structural Materials Properties Microstructure and Processing* 351 (1-2), 86-97.
- Beyerlein I. J., Lebensohn R. A., Tome C. N., 2003. Modeling texture and microstructural evolution in the equal channel angular extrusion process. *Materials Science and Engineering a-Structural Materials Properties Microstructure and Processing* 345 (1-2), 122-138.
- Beyerlein I. J., Li S., Necker C. T., Alexander D. J., Tome C. N., 2005. Non-uniform microstructure and texture evolution during equal channel angular extrusion. *Philosophical Magazine* 85 (13), 1359-1394.
- Biswas K., 2005. Comparison of various plasticity models for metal powder compaction processes. *Journal of Materials Processing Technology* 166 (1), 107-115.
- Carmai J. and Dunne F. P. E. 2004. Generalised constitutive equations for densification of metal matrix coated fibre composites. *Materials Science and Technology* 20(4), 478-484.
- Carmai J. and Dunne F. P. E., 2005. A model for the consolidation of hexagonal array matrix coated fibre composites. *Modelling and Simulation in Materials Science and Engineering* 13(6), 1005-1014.
- Carroll M. M., 1986. An Empirical-Model for Hot Isostatic Pressing of Metal Powders. *Metallurgical Transactions a-Physical Metallurgy and Materials Science* 17 (11), 1977-1984.
- Delo D. P., Piehler H. R., 1999. Early stage consolidation mechanisms during hot isostatic pressing of Ti-6Al-4V powder compacts. *Acta Materialia* 47 (9), 2841-2852.
- Duva J. M., Crow P. D., 1992. The Densification of Powders by Power-Law Creep during Hot Isostatic Pressing. *Acta Metallurgica Et Materialia* 40 (1), 31-35.
- Ferrasse S., Segal V. M., Hartwig K. T., Goforth R. E., 1997. Development of a submicrometer-grained microstructure in aluminum 6061 using equal channel angular extrusion. *Journal of Materials Research* 12 (5), 1253-1261.
- Ferrasse S., Segal V. M., Hartwig K. T., Goforth R. E., 1997. Microstructure and properties of copper and aluminum alloy 3003 heavily worked by equal channel angular extrusion. *Metallurgical and Materials Transactions a-Physical Metallurgy and Materials Science* 28 (4), 1047-1057.
- Gurson A. L., 1977. Continuum Theory of Ductile Rupture by Void Nucleation and Growth: Part I—Yield Criteria and Flow Rules for Porous Ductile Materials. *Journal of Engineering Materials and Technology* 99, 2-15.
- Haouaoui M., Karaman I., Maier H. J., Hartwig K. T., 2004. Microstructure evolution and mechanical behavior of bulk copper obtained by consolidation of micro- and nanopowders using equal-channel angular extrusion. *Metallurgical and Materials Transactions a-Physical Metallurgy and Materials Science* 35A (9), 2935-2949.
- Iwahashi Y., Horita Z., Nemoto M., Langdon T. G., 1997. An investigation of microstructural evolution during equal-channel angular pressing. *Acta Materialia* 45 (11), 4733-4741.
- Iwahashi Y., Horita Z., Nemoto M., Langdon T. G., 1998. The process of grain refinement in equal-channel angular pressing. *Acta Materialia* 46 (9), 3317-3331.
- Karaman I., Robertson J., Im J. T., Mathaudhu S. N., Luo Z. P., Hartwig K. T., 2004. The effect of temperature and extrusion speed on the consolidation of zirconium-based metallic glass powder using equal-channel angular extrusion. *Metallurgical and Materials Transactions a-Physical Metallurgy and Materials Science* 35A (1), 247-256.
- Karaman I., Haouaoui M., Maier H. J., 2007. Nanoparticle consolidation using equal channel angular extrusion at room temperature. *Journal of Materials Science* 42 (5), 1561-1576.
- Kim H. S., Seo M. H., Oh C. S., Kim S. J., 2003. Equal channel angular pressing of metallic powders. *Advanced Materials Processing* 11 437 (4), 89-92.
- Kim K. T., Carroll M. M., 1987. Compaction Equations for Strain-Hardening Porous Materials. *International Journal of Plasticity* 3 (1), 63-73.
- Kim K. T., Suh J., 1990. Model for Hot Compaction of Metal Powders. *Powder Metallurgy* 33 (1), 40-44.
- Li S., Bourke M. A. M., Beyerlein I. J., Alexander D. J., Clausen B., 2004. Finite element analysis of the plastic deformation zone and working load in equal channel angular extrusion. *Materials Science and Engineering a-Structural Materials Properties Microstructure and Processing* 382 (1-2), 217-236.
- Luis-Perez C. J., Luri-Irigoyen R., Gaston-Ochoa D., 2004. Finite element modelling of an Al-Mn alloy by equal channel angular extrusion (ECAE). *Journal of Materials Processing Technology* 153 (54), 846-852.

- Matsuki K., Aida T., Takeuchi T., Kusui J., Yokoe K., 2000. Microstructural characteristics and superplastic-like behavior in aluminum powder alloy consolidated by equal-channel angular pressing. *Acta Materialia* 48 (10), 2625-2632.
- Oh S. J., Kang S. B., 2003. Analysis of the billet deformation during equal channel angular pressing. *Materials Science and Engineering a-Structural Materials Properties Microstructure and Processing* 343 (1-2), 107-115.
- Olovsson L., Simonsson K., Unosson M., 2005. Selective mass scaling for explicit finite element analyses. *International Journal for Numerical Methods in Engineering* 63 (10), 1436-1445.
- Oruganti R. K., Subramanian P. R., Marte J. S., Gigliotti M. F., Amancherla S., 2005. Effect of friction, backpressure and strain rate sensitivity on material flow during equal channel angular extrusion. *Materials Science and Engineering a-Structural Materials Properties Microstructure and Processing* 406 (1-2), 102-109.
- Parasiris A., Hartwig K. T., Srinivasan M. N., 2000. Formation/consolidation of WC-Co cermets by simple shear. *Scripta Materialia* 42 (9), 875-880.
- Robertson J., Im J. T., Karaman I., Hartwig K. T., Anderson I. E., 2003. Consolidation of amorphous copper based powder by equal channel angular extrusion. *Journal of Non-Crystalline Solids* 317 (1-2), 144-151.
- Segal V. M., 1995. Materials processing by simple shear. *Materials Science and Engineering A* 197 (2), 157-164.
- Senkov O. N., Miracle D. B., Scott J. M., Senkova S. V., 2004. Equal channel angular extrusion compaction of semi-amorphous Al<sub>85</sub>Ni<sub>10</sub>Y<sub>2.5</sub>La<sub>2.5</sub> alloy powder. *Journal of Alloys and Compounds* 365 (1-2), 126-133.
- Senkov O. N., Senkova S. V., Scott J. M., Miracle D. B., 2005. Compaction of amorphous aluminum alloy powder by direct extrusion and equal channel angular extrusion. *Materials Science and Engineering a-Structural Materials Properties Microstructure and Processing* 393 (1-2), 12-21.
- Smith L. M., Ganeshmurthy N., Murty P., Chen C. C., Lim T., 2004. Finite element modeling of the tubular hydroforming process - Part 1. Strain rate-independent material model assumption. *Journal of Materials Processing Technology* 147 (1), 121-130.
- Stolyarov V. V., Lapovok R., 2003. Effect of backpressure on the structure and properties of Al-based alloys processed by ECAP. *Thermec'2003, Pts 1-5* 426 (4), 2825-2830.
- Tvergaard V., 1981. Influence of Voids on Shear Band Instabilities under Plane-Strain Conditions. *International Journal of Fracture* 17 (4), 389-407.
- Valiev R. Z., Langdon T. G., 2006. Developments in the use of ECAP processing for grain refinement. *Reviews on Advanced Materials Science* 13 (1), 15-26.
- Wilkinson D. S., Ashby M. F., 1975. Pressure Sintering by Power Law Creep. *Acta Metallurgica* 23 (11), 1277-1285.
- Xia K., Wu X., 2005. Back pressure equal channel angular consolidation of pure Al particles. *Scripta Materialia* 53 (11), 1225-1229.
- Yoon S. C., Kim H. S., 2006. Equal Channel Angular Pressing of Metallic Powders for Nanostructured Materials. *Materials Science Forum* 503, 221-226.
- Zhu Y. T., Lowe T. C., 2000. Observations and issues on mechanisms of grain refinement during ECAP process. *Materials Science and Engineering a-Structural Materials Properties Microstructure and Processing* 291 (1-2), 46-53.